FIBER VOLUME FRACTION AND DISTRIBUTION IN THERMOPLASTIC COMPOSITES FOR IN-SITU AFP

Yannick T. Schäfer[1], Ashley R. Chadwick[1]

[1]Institute of Structures and Design, German Aerospace Center (DLR),
Pfaffenwaldring 38-40, 70569 Stuttgart, Germany
Email: yannick.schaefer@dlr.de, Web Page: https://www.dlr.de/en/bt

Keywords: Fiber Volume Fraction, in-situ AFP, Thermoplastic Composites, Microscopy

Abstract
Thermoplastic in-situ Automated Fiber Placement promises advantages in cost and manufacturing time for large composite structures. With this technology, the consolidation quality depends on both process parameters and prepreg tape composition. In this paper, an automated digitized analysis tool based on micrographs is presented and applied to a selection of commercial prepreg materials and laminates manufactured with in-situ AFP and additional consolidation. The tapes are analyzed with respect to fiber volume fraction and distribution, thickness, porosity and surface roughness, allowing predictions for the in-situ suitability. Significant variations are found between manufacturers. The fiber fraction histograms reveal major deviations from the ideal fiber distribution. Microstructural characteristics are identified that may be used to assess the suitability for in-situ consolidation. This includes a thickness-wise fiber volume fraction distribution with matrix rich surfaces, as well as overall low porosity and surface roughness.

1. Introduction

With the continued and widespread implementation of composite materials for large aerospace applications, the industry aims towards a reduction in manufacturing time and cost. Thermoplastic in-situ Automated Fiber Placement (AFP) is a disruptive technology promising advantages over conventional autoclave based thermoset and thermoplastic composites, specifically a reduced manufacturing timeline [1]. With in-situ technology, consolidation is achieved in a small timeframe during the continuous process by pressing the heated tape to the substrate surface with a consolidation roller. With this limited combination of time, pressure and temperature, the process parameters have to be well defined in order to achieve a good consolidation and laminate quality [2, 3, 4]. In addition to the process parameters, the prepreg composition is a second major influence on the laminate quality. The consolidation process is based on a combination of intimate contact and molecular diffusion [5, 6, 7]. Previous studies have indicated that satisfactory intimate contact for in-situ AFP can be achieved when the prepreg exhibits low surface roughness and high surface resin content [8, 9]. Deviations from these respectively low and high expected values can result in interlaminar voids, reducing the performance of the final part. A recent study assessed the composition of various prepreg materials [9] and reported significant correlations between these prepreg properties and the resultant laminate porosity and mechanical strength, particularly the interlaminar shear strength (ILSS). Interlaminar porosity, i.e. voids exhibited within the prepreg material as part of the fiber-matrix impregnation process, is also known to persist to the final part, as the short heating cycle of AFP is not sufficient to completely remove voids before the matrix resolidifies following melting [9, 10, 11, 12]. This makes the avoidance of additional porosity in the interlaminar zone that much more important to ensure maximum part performance. Raps et al. (2024) proposed the fiber volume fraction distribution at the prepreg surface as a quantitative indicator of the surface resin content and as a criterion of AFP-suitability. However, the distribution of fibers through the full prepreg and eventual laminate thickness can provide additional insight into part

performance. As Figure 1 suggests, the actual fiber volume distribution may deviate significantly from the ideal uniform distribution and has been the topic of discussion in several studies [3, 4, 13]. Assadi (2021) reported great variations of microstructural tape composition between manufacturers and described the influence on the AFP process, however only on a qualitative level. As the fiber fraction distribution directly influences the distribution of thermal energy during the AFP process (through direct coupling with the near-infrared laser heat source), the interpretation of subsequent laminate thermal and mechanical properties (such as degree of crystallinity and tensile/compressive strength), and application-specific performance such as gas permeability (for hydrogen storage vessels), detailed information on this property is highly advantageous.

Within this work, a robust and repeatable tool is presented through which the fiber volume fraction (FVF) of unprocessed prepregs and finished laminates can be spatially resolved. This tool is applied to a broad range of prepregs from different commercial suppliers, assessing the FVF distribution and deviation from the nominal integral value. Additionally, surface roughness and porosity value are determined and taken into consideration for the evaluation of tape quality. The influence of manufacturing is briefly explored by comparing in-situ AFP laminates to press- and vacuum-consolidated AFP laminates.

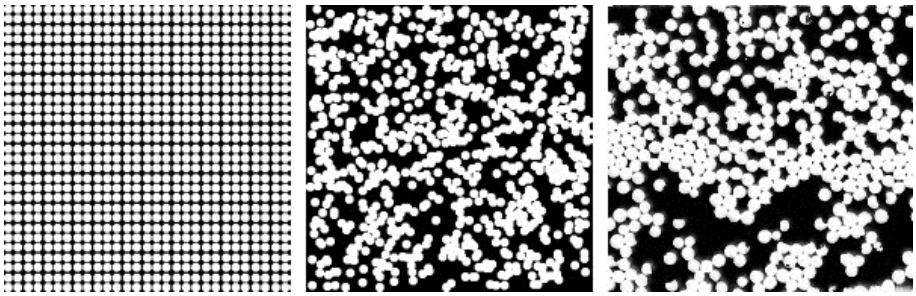

Figure 1. Ideal even (left), random (middle) and real (right) fiber distribution.

2. Methodology

The experimental section of this work is based on a selection of thermoplastic reinforced carbon fiber prepreg tapes and laminates manufactured from those tapes using Automated Fiber Placement with in-situ (IS) consolidation, as well as additional vacuum (VC) and hot-press (HP) consolidation. Table 1 provides an overview of the material selection. All tape material is unidirectional carbon fiber reinforced low-melt polyaryletherketone (LM-PAEK) except Tape E which uses PEEK.

Based on the previously discussed literature, a prepreg tape for in-situ AFP is expected to comply with specific microstructural composition requirements. This includes a low standard deviation of the FVF correlating to an even distribution of fibers in combination with a matrix-rich surface. This thickness-wise variation may be characterized by the fiber fraction distribution. Overall low porosity values are desirable. Additionally, the surface roughness was measured for comparison. The surface roughness is measured with a *Keyence VR-5000* 3D optical measurement system using the multiple line roughness analysis. The wavelength threshold values were set to λ_s = 25 µm and λ_c = 0.8 mm.

2.1. Microscopy

Micrographs are a standard methodology for microstructural analysis. Microscopy is a relatively fast and low-cost process. It is however limited in the volumetric depth of information which requires several samples for statistical compensation. While computed tomography (CT) is considered the most accurate and reliable method [14], the lower resolution and contrast between fibers and matrix limits the determination of the fiber volume fraction.

Table 1. Overview of the analyzed materials.

Specimen	**Matrix**	**State**	**Manufacturer**	**Nominal FVF [%]**	**Nominal Thickness [mm]**
Tape A	LM-PAEK	Unprocessed	M1	58.19*	0.20
Tape B	LM-PAEK	Unprocessed	M1	58.19*	0.20
Tape C	LM-PAEK	Unprocessed	M2	52.28*	0.17
Tape D	LM-PAEK	Unprocessed	M3	60.00	0.06
Tape E	LM-PEEK	Unprocessed	M4	57.00	0.06
Specimen	**Material**	**Consolidation**	**Manufacturer**	**Stacking**	
Laminate 1	Tape A	IS & HP	DLR	$[0, 45, 90, -45]_{2S}$	-
Laminate 2	Tape C	IS & VC	DLR	$[0, 45, 90, -45]_{2S}$	-
Laminate 3	Tape D	IS & VC	DLR	$[0, 45, 90, -45]_{2S}$	-

* Calculated from the fiber mass fraction with the nominal fiber and matrix density

In this work the method of analysis for tapes and laminates is based on micrographs of polished specimens analyzed with a *Keyence VHX-5000* digital microscope. Due to the thermoplastic matrix being sensitive to high temperatures, the specimens cannot be mounted in a hot-press procedure. Instead, a commercial epoxy system for polishing was used. Fully automated analysis of micrographs requires a strong contrast between the specimen and the mounting material. To achieve this, 5 wt% of white coloring (Universal Colour Paste Signal White (RAL 9003)) was added to resin. To the naked eye, the cured resin appears perfectly white. A microscope however only picks up a light gray color unsuited for automated separation. This can be altered by using bright field microscopy under fully polarized light. The specimen will at first appear very dark, but increasing the light intensity to the absolute maximum of the camera reveals the original colors similar to the unpolarized view, while the mounting resin is outshined to pure white. This allows for automated detection of the specimen surface using grayscale thresholding. For automated scale detection, the scale bar was colored black and positioned at the lower right corner of the image. Laminate material specimens were mounted in a conventional way using clear resin as the surface detection is less relevant due to the larges sample size.

Preparation of the specimens for microscopy consists of a five-step grinding and polishing process in a semi-automatic *Struers TegraPol-31* polishing machine. The samples were ground with 220 and 550 grit SiC paper followed by 9 µm, 3 µm and 0.25 µm diamond suspension for polishing. In between the process steps, an ultrasonic cleaning procedure in plain water was used to prevent scratches from contamination with previous grit size particles.

2.2. Image Analysis

The image processing and analysis was done using a Python program. Based on the white-colored mounting material, fully automated analysis of the micrographs was achieved using the following procedure.

1. Scale Detection
   The micrograph is transformed to grayscale and inverted. The scale will appear white allowing thresholding of the scale only. Using the contour detection function of the Python *OpenCV* library, the scale is detected as the greatest linear length.
2. Thresholding Mounting Material
   The sample material can be distinguished from the mounting material using the *Triangle* threshold from the *scikit-image* library. Small errors and artefacts from the polishing process can be smoothed out with a median blur filter from *OpenCV*. Good results were achieved with a filter kernel size of 15 pixel. A coherent specimen surface is vital for the following processes. An additional iteration can be integrated if the surface is not sufficiently sharp. Using *Otsu's* threshold, the first and last pixels is detected. With this method, dry fibers on the surface tend to be undistinguishable from the mounting material resulting in local errors.

3. Image Cropping
   The position of the scale is detected by checking every line starting from the image bottom. The image is then cropped just above the scale to remove all artificial pixels
4. Porosity Detection
   As porosity usually appears darker compared to the sample, it may be thresholded with a *Max Entropy* algorithm. Median filtering is necessary to consolidate the pixels within a pore, as the base of the pores tend to reflect light resulting in non-black pixels. Filtering also reduces the amount of falsely detected artefacts, which are mostly small incoherent regions eliminated by the filter.
5. Image Rotation
   Correct even positioning of the specimen during microscopy is often inconvenient. The mean orientation of the specimen in the image can however be detected using the *OpenCV* functions *Canny* and *HoughLines*. The required angle of rotation is derived from the gradient of this linear fit. Additional cropping is required to exclude the triangular black corners which would hinder the following analysis.
6. Specimen Thickness Analysis
   From step 2 results an image showing all pixels corresponding to the specimen. The thickness of this sample can be calculated as the length between the first and last valid pixel multiplied with the scale factor. By determining this length for each column, a histogram of the specimen thickness can be derived.
7. Fiber Volume Fraction Distribution Analysis
   For the determination of a FVF histogram, discretization is necessary. The representative elementary volume is defined to 21 by 21 µm, which is equivalent to 3 fiber diameters. For each discrete area, a mask describing the indices of pixels corresponding to the specimen is derived. The grayscale image is thresholded using *Otsu's* algorithm to separate matrix and fibers. The fiber volume fraction is calculated as the pixel ratio for all valid pixels in the mask. From this, a histogram of FVF is derived as well as an overview image with false color representation.

The size of the representative elementary volume for the FVF distribution analysis is vital but difficult to define. Small values approaching 1 pixel will result in a binary distribution, while overly large values will produce averaged values without information about distribution of fibers. The ideal value shall reveal the existence of fiber- and matrix-rich regions, which are by definition larger than one fiber diameter. Therefore, the size was defined as three fiber diameters resulting in Gaussian-like distributions, which is considered reasonable and provides useful information of the standard deviation within a single sample. Similar conclusions may be derived from the nearest-neighbor distributions. These however require circle detection algorithms, which fail when the ply angle is either unknown or near 90°. The areal distribution without detection is therefore considered superior for laminate analysis, particularly when considering laminates with quasi-isotropic or cross-ply layups.

Figure 2 shows a representative analyzed cross-section of Tape A with the local fiber volume fraction as false color representation.

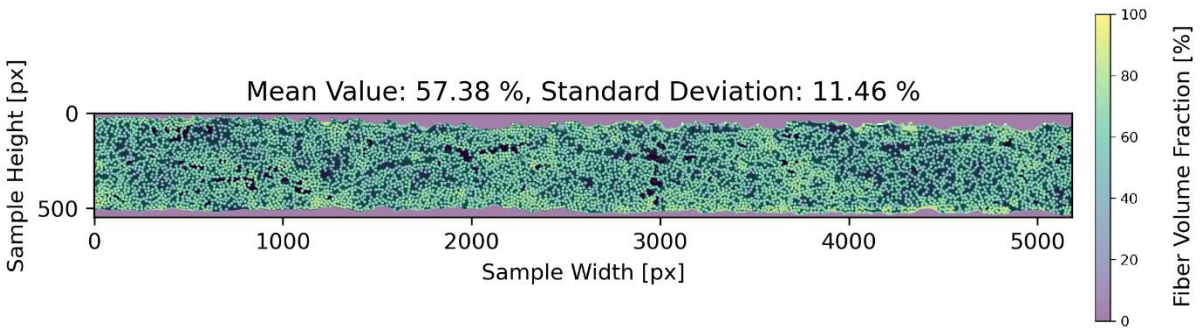

Figure 2. Fiber volume fraction false color representation

3. Results and discussion

An overview of the results is given in Table 2. As previously discussed in Section 2.2, the standard deviation of the fiber volume fraction is a local phenomenon. This value does not represent the deviation of integral values between several cross-sections, but gives insight into the fiber distribution and its deviation from an ideal even arrangement disclosing fiber- and matrix-rich areas. Figures 3 – 7 show the fiber volume fraction histogram and thickness-wise distribution for the selected tapes. Due to the small thickness of Tape E, the 21 µm discretization leads to an insufficient number of data points for the thickness-wise distribution. Therefore, a finer resolution of 7 µm is used to assess the distribution characteristics (Figure 7). Figures 8 and 9 show the shift in the fiber fraction histogram due to additional consolidation. Representative sections of the selected tapes are shown in Figure 10.

Table 2. Analysis result overview.

Specimen	FVF [%]	Thickness [mm]	Porosity [%]	Surface Roughness R_z [µm]
Tape A	55.12 ± 11.40	0.21 ± 0.01	1.57 ± 0.73	12.88 ± 1.91
Tape B	53.91 ± 13.09	0.22 ± 0.01	0.26 ± 0.47	17.87 ± 3.32
Tape C	43.69 ± 15.78	0.14 ± 0.02	0.99 ± 0.75	15.80 ± 3.38
Tape D	57.84 ± 13.97	0.07 ± 0.02	0.58 ± 0.68	15.29 ± 1.57
Tape E (7 µm res)	47.95 ± 25.02**	0.06 ± 0.00	5.97 ± 2.87	9.79 ± 3.31
Laminate 1 IS	60.45 ± 15.75	-	2.30 ± 0.75	-
Laminate 1 HP	62.28 ± 16.01	-	0.08 ± 0.02	-
Laminate 2 IS	52.62 ± 17.99	-	1.82 ± 0.59	-
Laminate 2 VC	53.73 ± 16.41	-	0.01 ± 0.01	-
Laminate 3 IS	55.19 ± 13.17	-	4.37 ± 2.98	-
Laminate 3 VC	55.15 ± 14.06	-	0.06 ± 0.06	-

** Including porosity

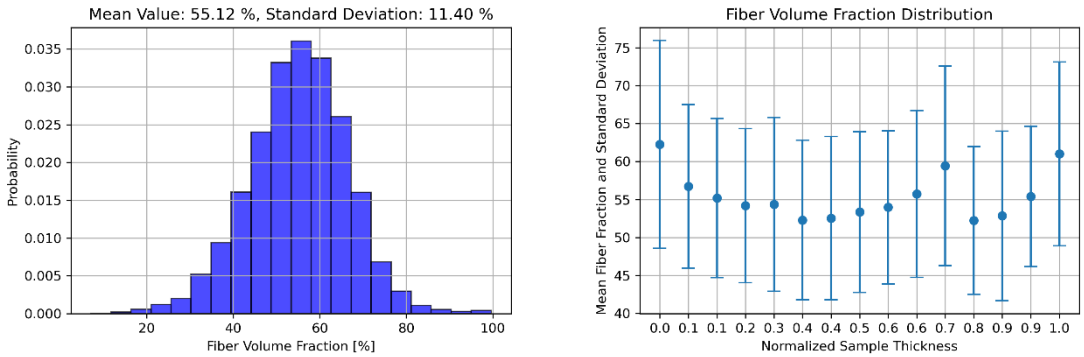

Figure 3. Tape A fiber volume fraction distribution

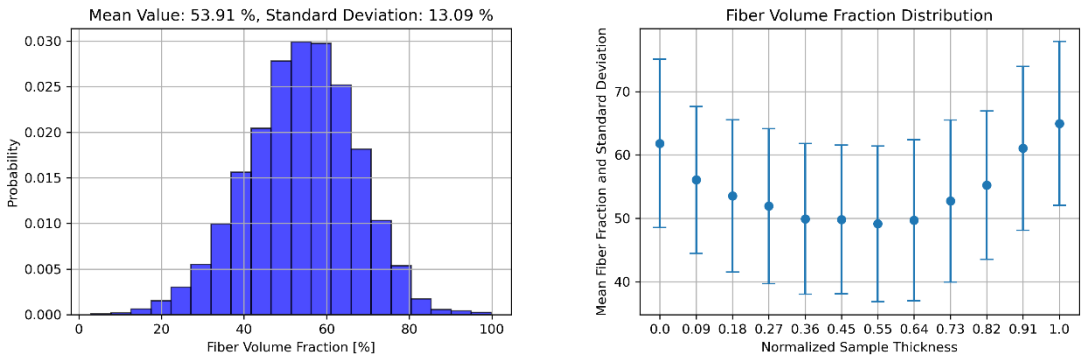

Figure 4. Tape B fiber volume fraction distribution

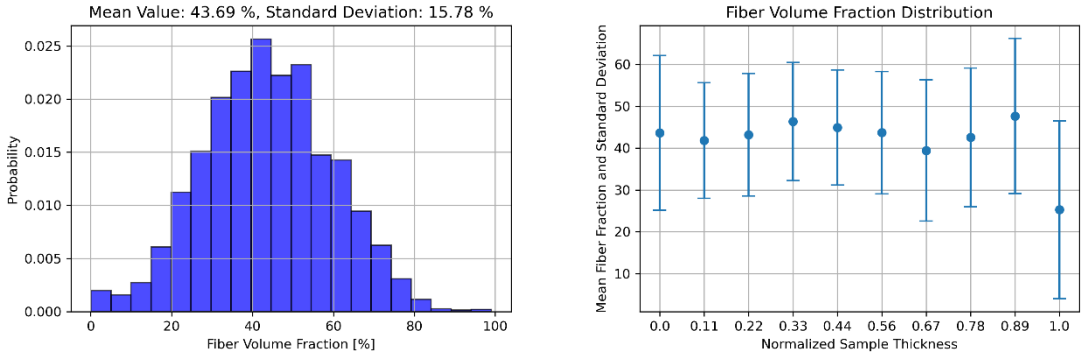

Figure 5. Tape C fiber volume fraction distribution

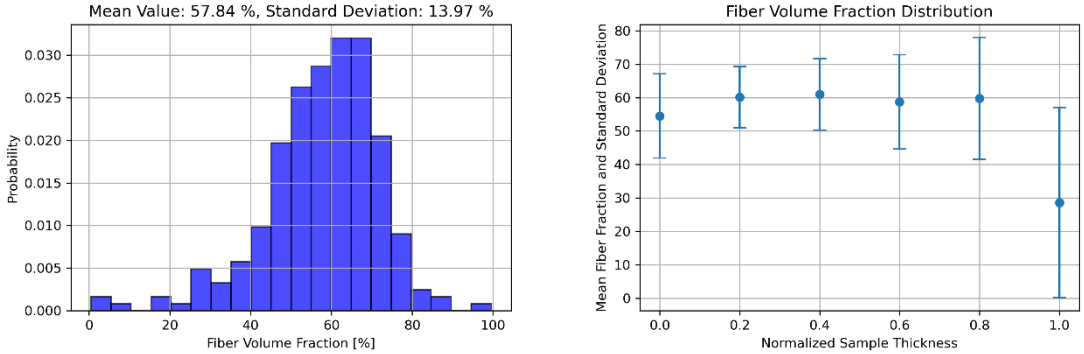

Figure 6. Tape D fiber volume fraction distribution

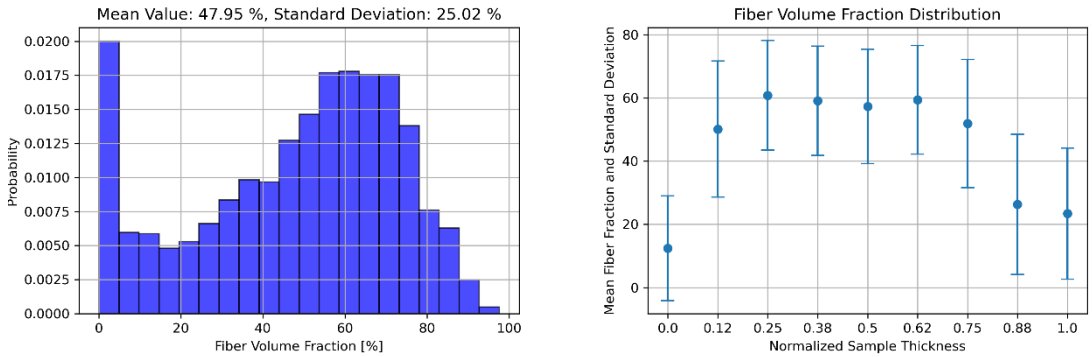

Figure 7. Tape E fiber volume fraction distribution with 7 µm discretization

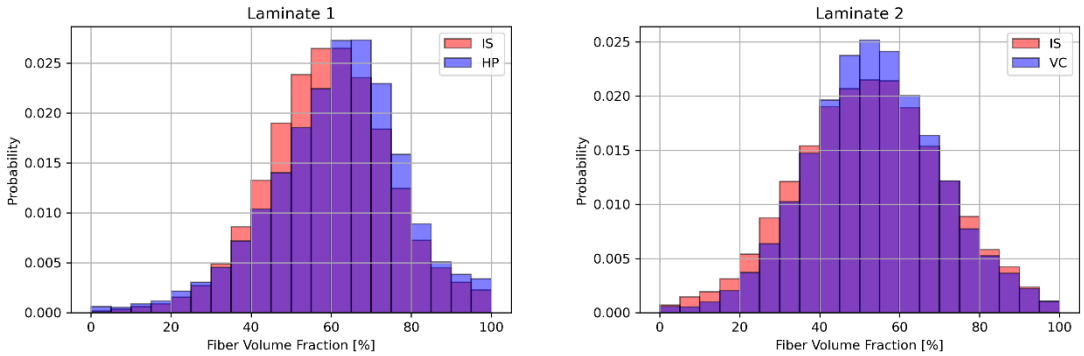

Figure 8. Fiber volume fraction shift with additional consolidation for Laminate 1 and 2

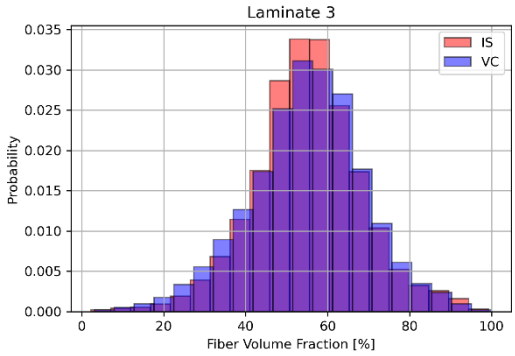

Figure 9. Laminate 3 fiber volume fraction shift

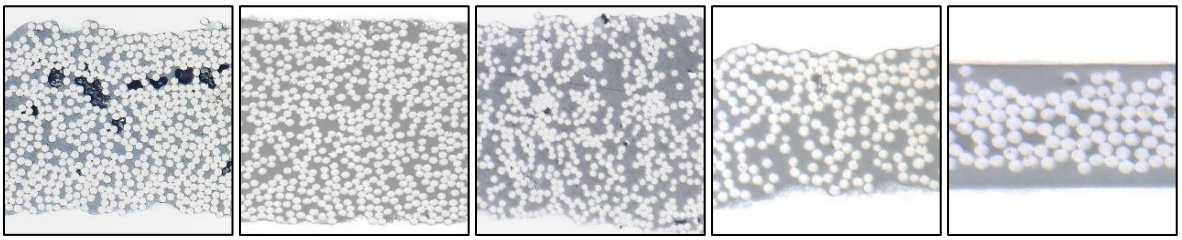

Tape A Tape B Tape C Tape D Tape E

Figure 10. Representative cross-sections of tapes A (left) to E (right)

The histograms depict the deviation of the fiber distribution. Ideal even distribution would lead to a single bin at the mean value, while the real distributions are spread out over the entire spectrum. Matrix-rich regions can be identified in Tapes C, D, and E as peaks near 0 % FVF. The resulting fiber volume fraction distributions through the tape thickness provide clear characteristics describing the surface resin content. Towards the surfaces, both Tape A and B show an increasing FVF, while Tape E provides a more favorable strong decrease, correlating with high consolidation potential. The distributions for Tapes C and D vary minimally over the prepreg thickness. Due to the process used to group FVF values by their through-thickness position, prepregs which exhibit significant variations in thickness result in inaccuracies in FVF prediction at the lower tape surface. Compared to the nominal values, the measured fiber fraction is slightly lower for all tapes, but significantly lower for Tape C and E. For Tape E, the automated porosity determination failed, thus the fiber fraction relates to the entire volume including the porosity. With Tape C, the optical impression from Figure 10 is that calculated value is correct for the selected specimen. However, the Laminate 2 manufactured from this tape was determined to be at approximately 53 %, close to the nominal value. As specimens were selected from the beginning of several spools, it is possible that the deviation is due to a systematic production error. With the white resin method, insufficiently white mounting resin may appear close to the tape surface due to lighting and polishing issues, resulting in incorrect surface fiber volume fraction and thickness measurements. With tapes, the micrograph quality is often inferior to laminates because the larger fraction of softer mounting material is worn faster than the specimen, resulting in a relief-like surface.
In terms of porosity, Tape B and D are superior, while Tape C is most desirable with respect to surface roughness. The analysis of laminates suggests that additional consolidation slightly increases the FVF. A significant shift in fiber distribution is not noticeable. A minor shift is detectable in the region of very low FVF due to the forming of resin-rich areas in the interply zone. The degree of porosity is significantly reduced by both vacuum and hot-press consolidation.

4. Conclusions

In this paper, a sophisticated tool was demonstrated for the quantitative analysis of prepreg tapes and laminates. In a broad study of different materials, significant deviations in tape composition and quality were found between manufacturers. The resulting data provides clear characteristics that may be used

to quantify the suitability of tapes for in-situ AFP. The methodology is however sensitive to the micrograph quality. Uneven lighting or brightness and polishing artefacts are common issues.
More data is required to fully correlate the tape characteristics with laminate quality. In the future, laminates will be manufactured from all selected tapes. Quantitative mechanical and microstructural analysis will likely help defining prepreg requirements for high quality in-situ AFP.

Acknowledgments
The results presented here were achieved within the NATURE (FKZ: 20W2208B) and ZEUS (FKZ: 20W2106C) research projects in the framework of the Federal Aviation Research Programme VI-2, funded by the Federal Ministry for Economic Affairs and Climate Action, on the basis of a decision by the German Bundestag.

References

[1] G. Marsh, "Automating aerospace composites production with fibre placement," *Reinforced Plastics,* vol. 55, pp. 32-37, 2011.

[2] I. Mössinger, L. Raps, D. Fricke, J. Freund, M. Löbbecke and A. R. Chadwick, "Characteristics of in-situ automated fiber placement carbon-fiber-reinforced low-melt polyaryl ether ketone laminates part 1: Manufacturing influences," *Journal of Composite Materials,* 2024.

[3] M. D. Assadi, "High Speed AFP Processing of Thermoplastics," *SAMPE Journal,* vol. 57, 2021.

[4] E. Oromiehie, A. K. Gain and B. G. Prusty, "Processing parameter optimisation for automated fibre placement (AFP) manufactured thermoplastic composites," *Composite Structures,* vol. 272, p. 114223, 2021.

[5] V. Agarwal, R. L. Mccullough and J. M. Schultz, "The Thermoplastic Laser-Assisted Consolidation Process-Mechanical and Microstructure Characterization," *Journal of Thermoplastic Composite Materials,* vol. 9, pp. 365-380, 1996.

[6] G. S. Springer, "Manufacturing Thermoplastic Matrix Composites," 1988.

[7] P. H. Dara and A. C. Loos, "Thermoplastic Matrix Composite Processing Model," 1985.

[8] M. B. Gruber, I. Z. Lockwood, T. L. Dolan, S. B. Funck, J. J. Tierney, P. Simacek, J. W. Gillespie Jr, S. G. Advani, B. J. Jensen, R. J. Cano and others, "Thermoplastic in situ placement requires better impregnated tapes and tows," in *Proceedings of the 2012 SAMPE conference and exhibition, Baltimore, MD,* 2012.

[9] L. Raps, A. R. Chadwick, I. Mössinger, M. Vinot, T. Behling and Y. Schaefer, "Characteristics of in-situ automated fiber placement carbon-fiber-reinforced low-melt polyaryl ether ketone laminates part 2: Effect of prepreg composition," *Journal of Composite Materials,* vol. 58, pp. 1523-1535, 2024.

[10] S. Ranganathan, S. G. Advani and M. A. Lamontia, "A Non-Isothermal Process Model for Consolidation and Void Reduction during In-Situ Tow Placement of Thermoplastic Composites," *Journal of Composite Materials,* vol. 29, pp. 1040-1062, 1995.

[11] M. A. Khan, P. Mitschang and R. Schledjewski, "Tracing the Void Content Development and Identification of its Effecting Parameters during in Situ Consolidation of Thermoplastic Tape Material," *Polymers and Polymer Composites,* vol. 18, pp. 1-15, 2010.

[12] M. A. Lamontia, M. B. Gruber, J. J. Tierney, J. W. Gillespie Jr, B. J. Jensen and R. J. Cano, "In situ thermoplastic ATP needs flat tapes and tows with few voids," in *30th international SAMPE Europe conference, Paris,* 2009.

[13] A. J. Comer, D. Ray, W. O. Obande, D. Jones, J. Lyons, I. Rosca, R. M. O. Higgins and M. A. McCarthy, "Mechanical characterisation of carbon fibre–PEEK manufactured by laser-assisted automated-tape-placement and autoclave," *Composites Part A: Applied Science and Manufacturing,* vol. 69, pp. 10-20, 2015.

[14] J. E. Little, X. Yuan and M. I. Jones, "Characterisation of voids in fibre reinforced composite materials," *NDT & E International,* vol. 46, pp. 122-127, 2012.